Study of Geomorphic Features of Noachis Terra, Mars: An Insight to Martian Tectonic Processes

Summary

By

KEYUR DE

Registration Number: R-14RS15210050

PRESIDENCY UNIVERSITY
KOLKATA

Supervisor:

Dr. Nilanjan Dasgupta

Contents

1. Introduction 2
2. Origin of the Problem 3
3. Geological Set Up of the Area of Study 3
4. Objective of the Study 4
5. Methodology 4
6. Observations: 5
    6.1. Crater Characterisation 6
        6.1.1. Polygonal Impact Craters 6
        6.1.2. Layered Ejecta Craters 7
    6.2. Deformation Signatures 7
        6.2.1. Compressional Structures 8
        6.2.2. Extensional Structures 9
    6.3. Pit-Crater Chain (PCC) 11
    6.4. Channels 12
        6.4.1. Cross-Correlation Analysis 13
        6.4.2. t-test 14
        6.4.3. Orientation Analysis 15
7. Discussions and Conclusions Drawn So Far 15

Tables *A*

Figures *i-xiii*

References 19-27

1. Introduction

Surface of Mars preserves evidences of tectonic activities of geological past. The cessation of tectonic activity at an early age followed by less rigorous surface processes compared to that on earth preserves geo-tectonic activity fossilised in its crust. This renders Mars as a natural laboratory to provide insight to crustal scale deformation and tectonics in the juvenile stages of the terrestrial planets.

Earth and Mars have many geomorphic features in common, however, Mars retains traces of early tectonic processes as old as 4.0 Ga (Grott et al., 2007; Williams et al., 2008; Xiao et al., 2012), while on earth later geological processes have recycled and removed such early tectonic imprints generated in its primordial conditions. This research aims to study Noachis Terra, a part of southern highlands of Mars (Figure 1), which preserves such tectonic structures. The satellite-based investigations in the area indicate the presence of local younger units surrounded by older basement rocks.

Geomorphologically Mars is divided into two physiographic provinces; the northern lowlands and the southern highlands (Watters and Schultz, 2010; Wilhelms and Squyres, 1984). Basalt floored (Wyatt and McSween, 2002) northern lowlands is believed to be younger than southern highlands. The boundary between these two contrasting topographic regions is known as dichotomy boundary. Noachis Terra, the area of current research, is a part of the southern highlands. This vast highland terrain is bordered to its west by Tharsis province, an enormous volcano-tectonic province; to its east by Hellas Planitia, a gigantic impact basin; and to its north-west by Valles Marineris a large canyon system. The area of present research is thus juxtaposed by tectonically and geomorphologically contrasting terrains, and still remains relatively unexplored compared to the adjacent tectonic blocks (Banerdt et al., 1982; Wilson and

Head, 2002; Witbeck et al., 1991; Lucchitta et al., 1992). This research work is aimed to understand the geological history of Noachis Terra from its various surface tectonic features and will draw its temporal and tectonic correlation from the structure-tectonics of the adjacent terranes.

2. Origin of the Problem

Noachis Terra (Figure 2) appears to have a very rugged cratered surface and preserves tectonic features such as grabens and wrinkle ridges. Surface of the Terra consist of oldest Noachian to youngest Amazonian units and therefore is a potential region for preservation of tectonic history of the entire areologic timescale. Geomorphic features are presented in Tanaka et al. (2014) on a regional scale. It is felt that documentation of finer details of these features are needed as they provide detailed information on their origin and evolution both temporally as well as tectonically, thereby helping to understand the processes that operated in Noachis Terra.

3. Geological Set Up of the Area of Study

The area of study is primarily comprised of Noachian aged (~>4.0 to ~3.74 Ga, oldest) (Mangold et al., 2012) massive basement rocks; two-thirds of which is of middle Noachian highland unit (~3.97 to ~3.86 Ga). At some regions within the Noachis Terra, the highland units are superimposed by Amazonian-Hesparian impact unit (~3.74Ga to recent) (Tanaka et al., 2014). Noachian crust is primarily basaltic (low Ca-pyroxene, olivine rich) (Mustard et al., 2005) with widespread occurrences of phyllosilicates. Noachis Terra records both compressional and extensional structures; eastern part is dominated by large scale extensional grabens and long linear ridges. In the western part, wrinkle ridges are seen along with strike slip faults (Schultz, 1989). Channels are mostly concentrated in the northern part of Noachis Terra near the mid-

latitude region (Tanaka et al., 2014). Presence of polygonal impact craters are also documented indicating influence of Argyre impact (Öhman et al., 2008).

4. Objective of the Study

The main objective of the present research is to establish the evolutionary history of local, regional and global scale tectonic elements of Noachis Terra and to find out their relation with general Martian tectonics. This would eventually help in understanding early tectonic processes operative on Mars and draw comparisons with the juvenile stages of the earth.

5. Methodology

This research work aims to delineate the tectonic elements of the area in finer scale, preparation of local to regional scale map and to establish the tectonic evolution of the region. Different geomorphological and structural elements are primarily identified from different images like Mars Orbiter Laser Altimeter (MOLA) colorized elevation map (resolution: 463 m/pixel; Smith et al., 2001), Thermal Emission Imaging System (THEMIS) - Infrared Day Global Mosaic (resolution: 100 m/pixel; Christensen et al., 2004; Edwards et al., 2011). Minute details of the geomorphological features and structures were studied from High Resolution Stereo Camera (HRSC) images (resolution: 25 m/pixel; Jaumann et al., 2007; Neukum and Jaumann, 2004), Context Camera (CTX) images (resolution: 6m/pixel; Malin et al., 2007) and High Resolution Imaging Science Experiment (HiRISE) images (resolution: 0.3m/pixel; McEwen et al., 2007). Important geomorphological features and structural elements were digitized on THEMIS-IR Day Global Mosaic as it portrays the feature prominently and display the entire area so that all the features can be mapped without any gap in QGIS 2.14.12 and JMARS (Christensen et al., 2009). Mosaic of CTX images were

used to map few features with minute details. MOLA colorized elevation map has been used to understand the general slope of the terrain.

Topographic sections extracted from MOLA DEM (Digital Elevation Model) (resolution: 463 m/pixel; Smith et al., 2001) and HRSC MOLA Blended DEM (200 m/pixel; Fergason et al., 2018), were considered to understand the subsurface structures following established methods (Schultz, 2000; Watters and Robinson, 1997; Montesi and Zuber, 2003). Several structural models were prepared using these sections. To understand the palaeostress conditions responsible for formation of grabens and wrinkle ridges, orientations of fault planes and slip directions of the fault planes (Golombek et al., 1996; Ferrill et al, 2004; Wyrick et al., 2004) were measured in image analysis software (Inkscape 0.91) and analysed using T-Tecto 3.0 (Žalohar, 2009) opensource software.

Trends of different segments of linear geomorphological and structural features were measured and plotted in rose diagrams using GEOrient 9.2 (Holcombe, 2005) to assess the dominant orientations.

In due course of study, channels with similar planforms are observed. The degree of similarity between these channels were further checked by cross-correlation method (Davis, 2002; Telatovich, 1998; Güneralp and Rhoads, 2005). Significance of cross correlation coefficients was then assessed by a simple one tailed t-test (Davis, 2002) at both 95% and 97.5% confidence levels.

6. Observations

Noachis Terra was divided into four domains for the present research (Figure 2), each of which has characteristic structural types; (i) *Domain I*, east of Coprates Rise, the

western end of Noachis Terra; (ii) *Domain II*, eastern part of Noachis Terra near Terra Sabaea region; (iii) *Domain III*, Pyrrhae Regio in the north-western part of the Terra and (iv) *Domain IV*, Pyrrhae Fossae area in north-western part. Observations from these regions are described in the following subsections:

6.1. Crater Characterisation

Geologically Noachis Terra is a very old terrain and thus heavily engraved with small to large impact craters. Crater morphology is studied in different zones of the study area. In general, the diameter of the craters ranges from few hundred meters to roughly 500 km. Both simple and complex types of craters are present. Craters with distinct morphology are studied in detailed:

6.1.1. Polygonal Impact Craters

Often craters do not have a circular outline, instead, they partially or wholly resemble a polygon having straight rim segments with "discernible" angles between them; these craters are known as Polygonal Impact Craters (PICs) (Korteniemi and Öhman, 2014). PICs are relatively more common in older geologic units i.e., Noachian cratered plains (Öhman et al., 2008), as in the present study area. Such polygonal shapes are due to the presence of pre-existing structures like faults or other similar planes of weakness having depths of ~100 to 1000 m prior to impact (Aittola et al., 2007, 2010; Eppler et al., 1983; Öhman et al., 2005, 2008; Watters et al., 2011, 2017).

Pyrrhae Fossae Region (Domain IV):

Seventeen craters (C_1 to C_{17}, Figure 3 of De et al., 2018) with distinct polygonal outlines were mapped and measured on THEMIS-IR Day Global Mosaic from *Domain IV*, Pyrrhae Fossae region. These craters are further classified into simple and

complex types (Table 1 of De et al., 2018) (Eppler et al., 1983; Gault et al., 1968; Öhman et al., 2008; Poelchau et al., 2009). Rose plot (Figure 5a of De et al., 2018) of the trends of the crater outlines of straight rim segments of the PICs show that NE-SW is the most frequent trend followed by a distinct NW-SE trend. Another peak in E-W direction is present in the rose diagram of PIC rim segments. So, it can be surmised that a set of pre-existing fractures predominantly along NE-SW with some NW-SE trending ones were present which helped to sketch the outline of the crater rims.

6.1.2. Layered Ejecta Craters

Layered ejecta craters are the most common ejecta morphology in Mars. These craters are surrounded by one or more layers of ejecta blankets with long runout flows or lobe like ramparts (Li et al. 2015).

The discernible layered ejecta craters have been studied in different domains (I, III, IV, Figures 3a, b and c) of the research area (Table 1). It is seen that the diameter of these craters are within 2-45 km. The study has been carried out on THEMIS-IR daytime global mosaic. It is observed that the most common type of layered ejecta craters are Single Layered Ejecta craters (Table 1).

6.2. Deformation Signatures

Noachis Terra show many prominent geomorphic deformation signatures like graben, wrinkle ridges, which may act as clues to decipher the tectonic processes responsible for their formation. Eastern part of the area has experienced major crustal extension as three large crustal scale grabens trending ~NNE-SSW are present here (De et al., 2014; Ruj et al., 2016, 2017). Westernmost corner of Noachis Terra, close to Coprates Rise (*Domain I*), has mainly experienced compressive tectonism as many wrinkle

ridges are present in this region. Several small-scale grabens are present near the margin with Margaritifer Terra in the North.

6.2.1. Compressional Structures

Amongst the compressional structures, wrinkle ridges are the most prominent one on the Martian surface. Characters of wrinkle ridges mapped and studied in the different domains of the study area are elaborated below:

East of Coprates Rise (Domain I):

In the north-western corner of Noachis Terra, near Coprates rise, two sets of wrinkle ridges trending N-S to NNE-SSW and NW-SE are present of these, closely spaced N-S to NNE-SSW trending set wrinkle ridge is the most prominent one (Figure 4). In general wrinkle ridge concentration in this area is very high and therefore they are closely spaced. The profile sections across the wrinkle ridges (Figure 5a, b, c), extracted through MOLA DTM, show that they all have asymmetrical profiles, with the base of western limb of the folded surface at higher elevation than that of eastern limb. Many of these wrinkle ridges persist upto a length of ~170kms without any break. These are ~5 to ~17 km wide and have an elevation offset of ~20 to ~130m. Palaeostress analysis using T-Tecto software reveal (Figure 5d) that SSE-NNW directed sub-horizontal maximum principal stress (σ_1) and corresponding sub-vertical minimum principal stress (σ_3) is responsible for generating the N-S to NNE-SSW trending wrinkle ridge set.

A set of prominent E-W to ENE-WSW trending linear ridge is also present in the region. Within the area of study it is seen that these ridges have displaced the NNE-SSW trending wrinkle ridges along their strike (Figure 5a).

Pyrrhae Fossae Region (Domain IV):

N-S trending widely spaced wrinkle ridges are present near Pyrrhae Fossae (Figure 6a). Approximately twenty three such wrinkle ridges were mapped, which were found to be ~10 to ~80 km in length, and ~4 to ~15 km in width. Conspicuously the density of wrinkle ridges of this domain is found to be much lower than those found in *Domain I*. Profile sections across such ridges (Figure 6b and c) show elevation offset ranging from ~50m to ~100m with western limb at higher elevation in most of the wrinkle ridges.

6.2.2. Extensional Structures

Extensional grabens of different dimensions are present throughout Noachis Terra. In the eastern part of the study area, in *Domain II*, very large-scale grabens (of hundreds of kilometres long) are present, while in the central (*Domain IV*) and western (*Domain III*) part regional scale narrow grabens or fossae (tens of kilometres long) are present. Detailed description of the grabens studied are given in following subsections:

Eastern part of Noachis Terra (Domain II):

On the west of the Hellas Planitia, i.e. in the eastern part of the Noachis terra, three NE-SW trending grabens are present (Figure 7a, b, c and d). The grabens are ~60-100km wide and the longest graben is ~1000km long. Floors of the grabens are at ~500m to ~900m depth with respect to the adjacent ground level (De et al., 2014). The graben boundaries are overprinted by numerous impact craters and therefore, appear to be discontinuous (Figure 7a). Even the graben floors are intensely cratered which indicates to their formation in the early stage of Martian crustal history (cf. Watters and Schultz, 2010). The Crater Size Frequency Distribution measurements

indicate the model age of the grabens as 3.84 (+0.022/-0.026) Ga (Ruj et al., 2018). Cross-sections across the grabens (Figure 7b) drawn on the basis of the topographic profiles derived from MOLA DTM show a series of horst and grabens resembling basin and range structure (Figure 7c) (De et al., 2014). The palaeostress analysis through T-TECTO software has been carried out to understand the stress regime responsible for formation of the grabens reveals a NW-SE trending maximum tensile stress (Figure 7d) (De et al., 2014).

Pyrrhae Regio (Domain III):

Several ~E-W trending narrow graben or fossae are present (Figure 8a and b) in the northern part of Noachis Terra, in Pyrrhae region (near the southern boundary of Margaritifer Terra and eastern end of Valles Marineris, Figure 1). MOLA profile sections reveal (Figure 8c and d) that these fossae are ~50m to ~900m deep and upto ~15km in width. Length of these fossae ranges from 10km to 150km. The palaeostress regime responsible for formation of these fossae are deduced. The slip vector analysis (Figure 8e) of these faults bounding these fossae, using T-Tecto software reveal a subvertical maximum principal stress (σ_1), and N-S trending sub-horizontal minimum principal stress (σ_3) direction.

Pyrrhae Fossae Region (Domain IV):

In the western part of Noachis Terra conspicuous E-W trending narrow grabens or fossae are present named Pyrrhae Fossae (Figure 1 of De et al., 2015a). There are eight fossae, ~20 to ~120km long and ~20 to ~170m deep as measured from the adjacent uplifted blocks. One such fossa (F_A), has transected through an unnamed crater (CR) situated at immediate south of the Pabo crater (23.1°W, 26.9°S, Figure 1 of De et al., 2015a). The CR has a circular rim, with no horizontal offset across F_A.

Structural profile of all the fossa has been prepared from the elevation data (Table 1 and Figure 2 of De et al., 2015a).

Profile sections across the channels of this region (Figure 2 of De et al., 2015a) indicate no elevation difference across them. Regular orientation of these grabens spread over an area of 140800sq km hint to a somewhat consistent internal stress regime responsible for development of the faults, represented geomorphologically as scarps that limit the grabens (Ferrill et. al., 2004; Wilson and Head, 2002). Fault slip analysis has been done using T-Tecto software to assess the palaeostress condition for formation of these grabens. The slip vector analysis of the set of these faults (Figure 2 of De et al., 2015a) bounding the grabens reveal a subvertical maximum principal stress (σ_1), and N-S trending sub-horizontal minimum principal stress (σ_3) direction (De et al., 2015a).

6.3. Pit-Crater Chain (PCC)

Pit-crater chains of two different trends, NW-SE (P_1) and WSW-ENE (P_2) are present within the westernmost graben (Figure 9a, b and c) of the graben set of *Domain II*, eastern part of Noachis Terra (Figure 7a). P_1 and P_2 are ~7km and ~20km long respectively and are at high angles to the NE-SW trending host-graben boundaries. Angle between the pit-crater chains is ~60^o which indicate to the possibility of being conjugate sets (De et al., 2014).

The presently studied PCCs do not match in disposition with previously reported chains by other authors (Wyrick et al., 2004) in the sense that they are at oblique to the host-graben margins. The P_1 and P_2 are neither along the graben margins nor are subparallel to them (De et al., 2014). From the disposition of these PCCs it is clear that their origin cannot be explained by the available models suggesting the structural setting for formation of pit-crater chains (Wyrick et al., 2004). With this study it is

proposed that these chains either were formed along a conjugate set of shear fractures (Figure 9d) in a completely separate stress regime, postdating the graben formation, where the minimum principal stress was NNE-SSW and intermediate principal stress was vertical (De et al., 2014).

6.4. Channels:

Channels, proposed as erstwhile pathways of water (Carr, 1996; Hynek et al., 2010; Mangold et al., 2004) are common on Martian surface. The courses of these channels are sometimes partially governed by the tectonic lineaments exposed on the surface (Kochel and Piper, 1986; Komatsu and Baker, 2007; Laity and Malin, 1985; Sharp and Malin, 1975). The area of study is covered with several regional scale channels (tens to hundreds of km) and very few global scale channels. Characteristics of the channels from different zones of the study area are given below:

Pyrrhae Regio (Domain III):

Morphological analysis show that the channels of this area show strong influence of regional structures on their pathways. Segments of few channels are parallel and at times share common path with the regional E-W trending fossae (Figure 10).

Pyrrhae Fossae Region (Domain IV):

Channels, present near Pyrrhae Fossae are quite interesting for their geometrical pattern, with a general trend of NNE/NE-SSW/SW (Figure 2a of De et al., 2018). THEMIS-IR Day Global Mosaic is used to map the channels in JMARS (Christensen et al., 2009); HRSC images were also studied for accurate observation and understanding of the surface features. For the analyses, lower order channels (Gravelius, 1914; Zavoianu, 1985), with simpler geometries were selected and digitized by drawing line appropriate with the scale of observation; channels with

dendritic (Zernitz, 1932) pattern were not considered. One of these channels (Y_6) is partially covered in a segment by a crater and its ejecta blanket; the channel path was marked by a dotted line at that part by joining a straight line at the points of intersection of the crater with the channel. Profile sections extracted (Figure 4 of De et al., 2018) from the HRSC MOLA Blended DEM across different segments of the studied channels reveal almost similarity in the elevations of opposite banks which indicate that they were not disrupted by any younger tectonic fabric along or sub-parallel to the channels. Moreover, within the area, the channels are also not seen to be intercepted by any tectonic fabric across them. Geometrical similarity of these channels have been tested statistically and the cause behind this similarity has been discussed in De et al., 2015b and De et al., 2018.

A. Cross -Correlation Analysis:

The cross-correlation analysis was done to group the channels showing statistical similarity of their courses, and to relate such groups to the existing tectonic fabric that was prevalent. For the analyses, a fixed reference axis i.e., a N-S trending axis is considered (Figure 2a of De et al., 2018), from which distances of the each match position (taken at 6 km interval) are measured (Table 2 of De et al., 2018) along E-W direction. Corresponding correlation coefficient (r_m) is calculated for each match position (Table 3 of De et al., 2018) for a particular channel with the other channels in the area. This exercise is repeated for all channels studied and mapped in the area (the collective data is listed in Table 3 of De et al., 2018).

The results (Table 3 of De et al., 2018) of the cross-correlation tests show that channels Y_1, Y_2, Y_3, Y_4, Y_5 and Y_6 yield high value of r_m amongst them while correlation of Y_7, Y_8, Y_9 and Y_{10} with other channels do not yield any significant

value. So, it can be surmised from the results discussed above, that the factor controlling the geometry of the channels Y_1, Y_2, Y_3, Y_4, Y_5 and Y_6 is different in nature from Y_7, Y_8, Y_9 and Y_{10} (De et al., 2018).

B. t-test:

Based on the r_m values obtained channels have been classified into two subgroups:

(a) *Subgroup I:* Channels with high positive r_m values indicating higher degree of similarity in their geometries.

(b) *Subgroup II:* Channels with low positive r_m values indicating lower degree of similarity in their geometries.

The statistical significance of cross-correlation coefficients was assessed by calculating 't' value of one tailed t-test (Davis, 2002) on a Null Hypothesis, exercised in a rejection mode.

The t-test was carried out with the Null Hypothesis as,

H_0: Channels with unique controlling factors do not show a match in t-test statistic.

The t-tests have been done amongst individual members of different subgroups. The t-test among the members of *subgroup I* (Table 4 of De et al., 2018) resulted in rejection of Null Hypothesis indicating that the channels, Y_1, Y_2, Y_3, Y_4, Y_5 and Y_6 have some statistical commonality among them. t-test values for members of *subgroup II* (Table 5 and 6 of De et al., 2018) does not fall in the critical region of rejection; thus channels Y_8, Y_9 and Y_{10} fail to show the statistical similarity amongst them (De et al., 2018).

C. Orientation Analysis:

The azimuths of the relatively straighter segments of the channels were mapped (Figure 3 of De et al., 2018) and their trends were considered for the preparation of the rose diagram (Figure 5b of De et al., 2018). Trends of the possible straight segments of the channels, plotted in the rose diagram, reveal that the most dominating trend is NE-SW (30˚-45˚) followed by NNE-SSW (15˚-30˚). Though the second major trend is NNE-SSW, there are two more minor peaks seen at NW-SE (substantial) and E-W (a few) directions (De et al., 2018).

7. Discussions and Conclusions Drawn So Far:

- Within the Noachis Terra, both extensional and compressional structures of different scales are present. Large scale compressional structures are mostly concentrated in western part of Noachis Terra, *Domain I* of our study area, while extensional structures are more prominent in the eastern part near *Domain II* (De et al., 2014).

- Wrinkle ridges near *Domain I*, east of Coprates Rise have formed due to SSE-NNW trending sub-horizontal maximum principal stress and corresponding sub-vertical minimum principal stress possibly generated by volcano-tectonic activity of Tharsis bulge, the huge volcano-tectonic province, present in the west of Noachis Terra.

- It was earlier proposed that the grabens on surface of Mars might have formed due to extension related to emplacement of dykes (Kortiniemi et al., 2006). Emplacement of these dykes is thought to have generated vertical maximum principal stress and corresponding horizontal extension responsible for

formation of normal fault bound Pyrrhae Fossae, present in the western part of Noachis Terra in *Domain IV* of our study region (De et al., 2015a).

- Crater concentration is very high in the region. Presence of polygonal impact craters in different localities indicate prominent influence of pre-existing regional structures on shaping crater outline. Statistical analysis of straight crater rims helped in understanding the orientation of dominant regional structures in *Domain IV*, Pyrrhae Fossae region, some of which are exposed while some are invisible (De et al., 2018).

- The channels of *Domain IV*, Pyrrhae Fossae region show similar planform. Degree of similarity between these channels is estimated through statistical analysis. This analysis reflects that some of the channels, have some statistical harmony while some have not. This research provides a statistical approach to identify the control of regional structures on channel course. The areal extent of the influence of these pre-existing tectonic lineaments is understandable from the statistical analyses as it is evident that the channels in the bordering regions of the study area do not show positive results. There may be control of other tectonic elements and/or topography on these channels (De et al., 2015b; De at al., 2018).

- Comparison between the rose diagrams of the straight segments of channels and PIC rims in *Domain IV*, Pyrrhae Fossae region reveal that they both have peaks in similar orientations. Most frequent trend in both channel and PIC rims is NE-SW, which is also the gross trend of the channels of the region. Both PIC rims and channels also have peaks in NW-SE and E-W orientation. These altogether indicate that dominant NE-SW and subordinate E-W trending

weak structural planes which possibly had their control on rim orientation of PICs as well as orientation of straight segments of the channels (De et al., 2018).

- **Chronology of Features:**

  - ***Domain III:***

    In the Pyrrhae Regio, outer rim of a very large sized crater (centred 29.4˚W, 17˚S) is transacted in a part by E-W trending fossae. Fluvial channel of the region originate from smaller polygonal impact crater ejecta, follows the E-W trending Fossae (A-F, Figure 8a) partially and terminates in the large crater. Polygonal impact craters present in the area reflect the existence of fractures pre-dating the PICs. Therefore the relative ages of the events can be summarised as:

	Channel formations Polygonal Impact Cratering Fossae and regional fracture formation Very Large Impact Crater (centred 29.4˚W, 17˚S)

  - ***Domain IV:***

    From the cross cutting relationships of the geomorphological features present in the available imagery, an attempt has been made to find their relative ages. In the Pyrrhae Fossae region, fluvial channel originating at Pabo crater, follows an N-S fracture, terminates at the Pyrrhae Fossa, F_A (Figure 1 of De et al., 2015a) and therefore clearly postdate the CR crater

and also the event of graben formation. Polygonal impact craters present in the area reflect the existence of fractures pre-dating the PICs. Relative ages of the events can be summarised as:

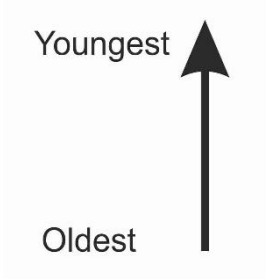	Palaeochannel formations Polygonal Impact Cratering Pyrrhae Fossae and regional fracture formation CR Crater Impact

- Lithospheric activity continued (extensional phase terminating ~3.8 Ga and compressional phase ~3.5-3.6 Ga; Ruj et al., 2018) shortly after two mega impact event, Hellas (3.99 Ga, Werner, 2008) and Argyre (3.93 Ga, Robins et al., 2013; or 3.83 Ga, Werner, 2008), mainly due to isostatic adjustment. In *Domain IV* (Figure 11a) of the study area, N-S trending maximum tensile stress (σ_3) (Figure 11b) generated E-W trending fossae possibly due to isostatic adjustment of Argyre mega impact around late Noachian time. In similar time, in *Domain II* (Figure 11a), isostatic adjustment of Hellas impact resulted in NW-SE trending maximum tensile stress (σ_3) (Figure 11b) and generated NE-SW trending large grabens. The stress regime changed into SSE-NNW directed (σ_1) (Figure 11b) compressional stress regime in *Domain I* (Figure 11a) during Early Hesperian time to generate NNE-SSW trending wrinkle ridges.

Table 1

Type of craters	Area		
	Domain IV: Pyrrhae Fossae Region	**Domain III: Pyrrhae Regio**	**Domain I: East of Coprates Rise**
SLE crater	58	26	69
DLE crater	5	3	12
MLE crater	3	8	7

Table 1: Number of different types of Layered Ejecta Craters studied in different regions of Noachis Terra (Figure 3a, b and c).

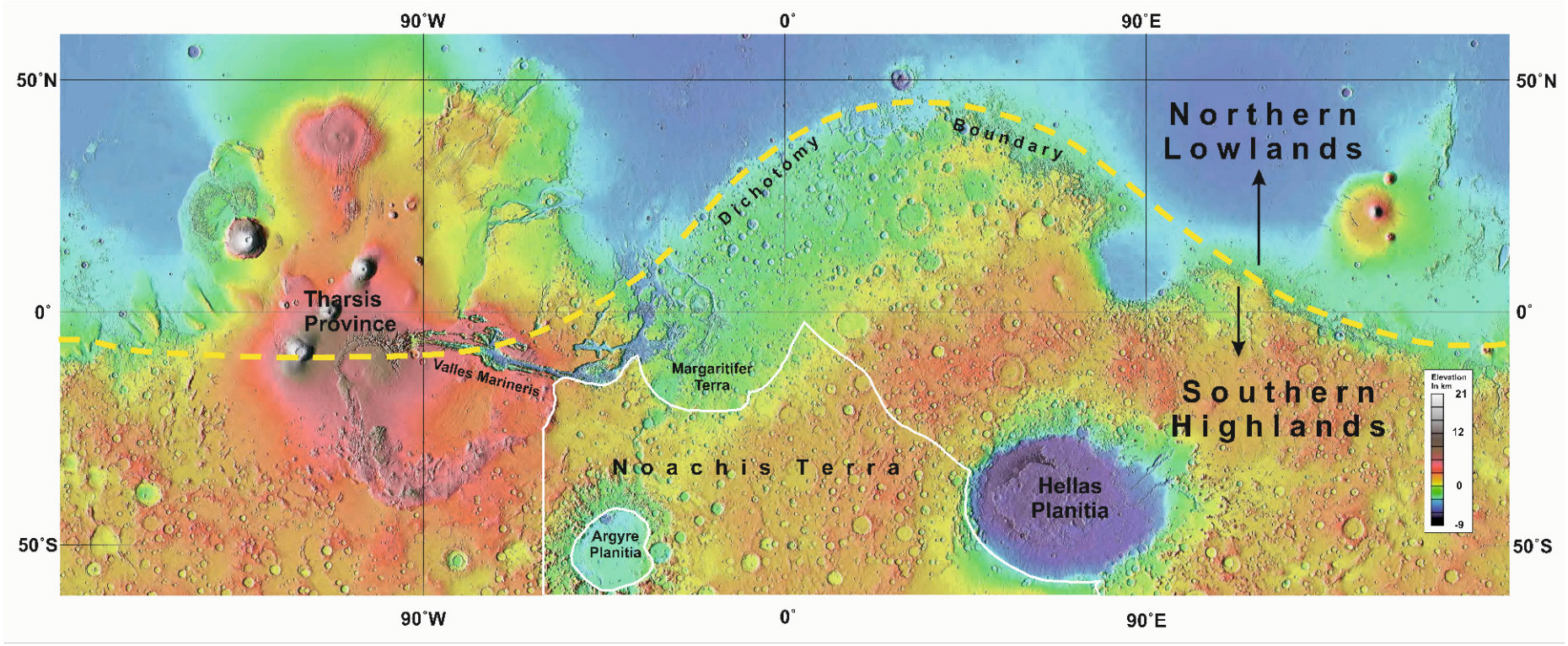

Figure 1: MOLA colourised elevation map showing different important provinces of Mars. Noachis Terra, the area of present research is marked by white line. Yellow broken line marks the global crustal dichotomy boundary.

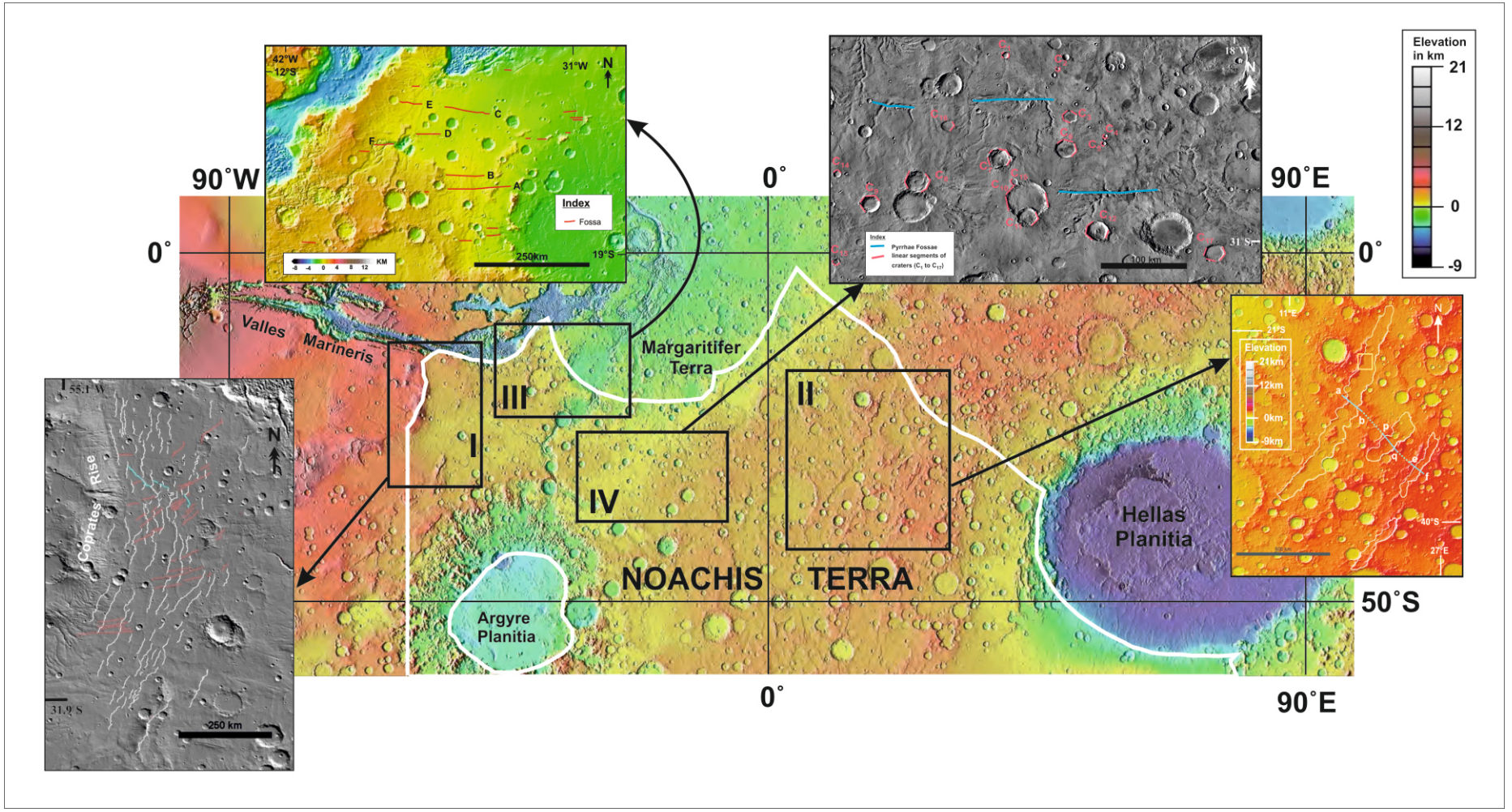

Figure 2: MOLA colourised elevation map showing locations of different domains studied in details. Domain I: east of Coprates Rise, Domain II: eastern part of Noachis Terra, Domain III: Pyrrhae Regio in the north-western part of the Terra and Domain IV: Pyrrhae Fossae area in north-western part.

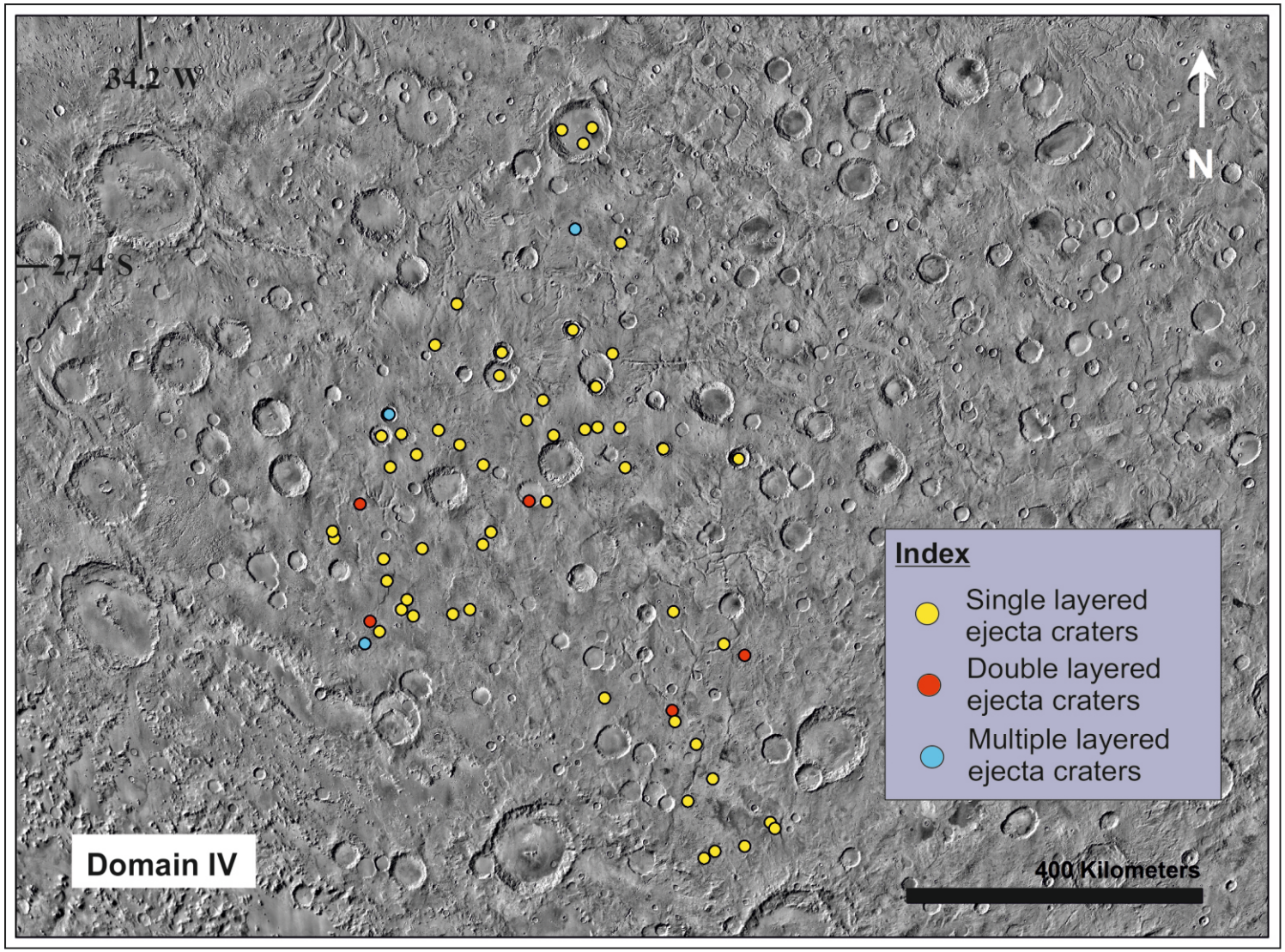

Figure 3a: THEMIS-IR Day Global Mosaic showing locations of different types of Layered ejecta crater in Domain IV.

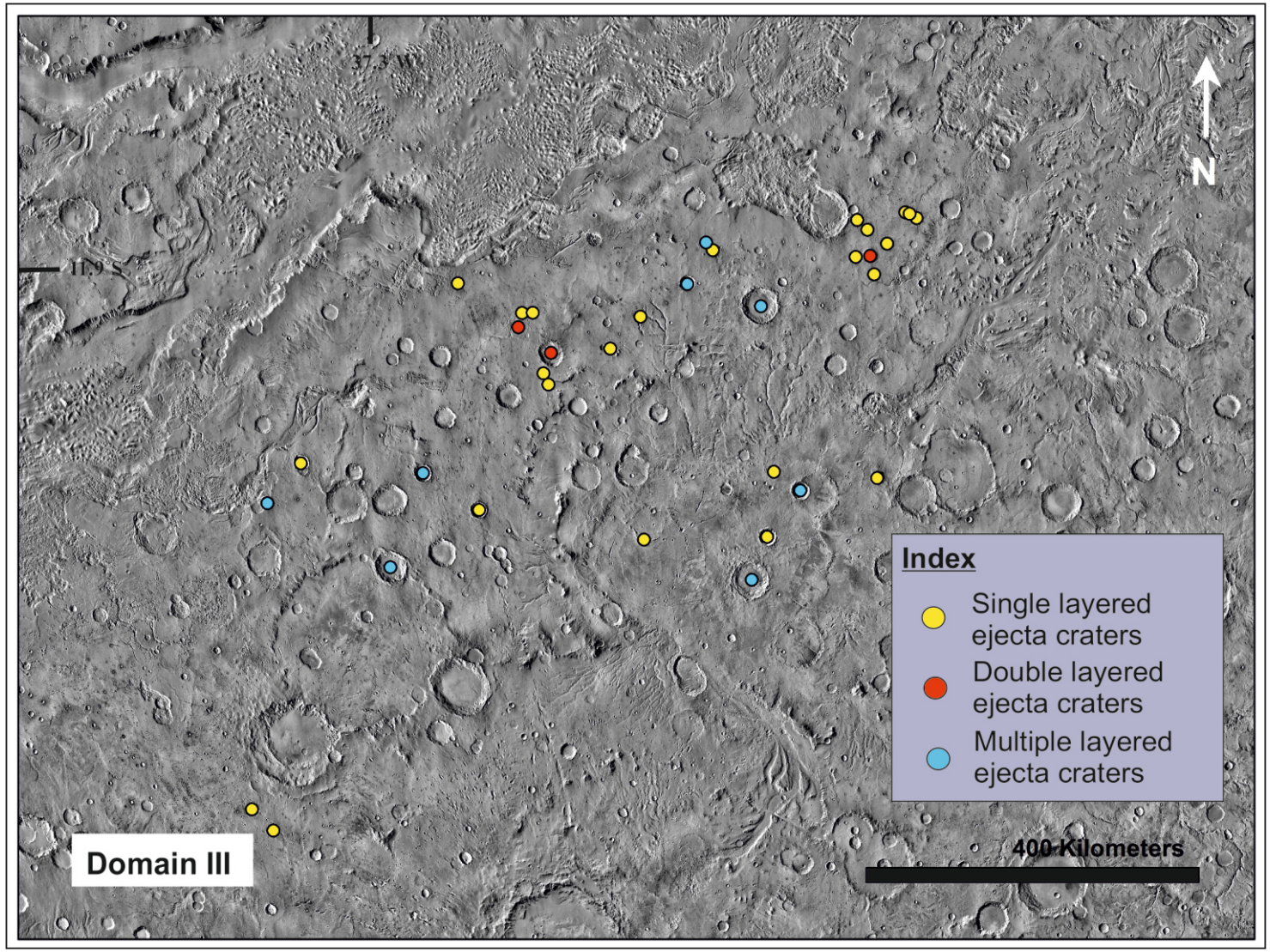

Figure 3b: THEMIS-IR Day Global Mosaic showing locations of different types of Layered ejecta crater in Domain III.

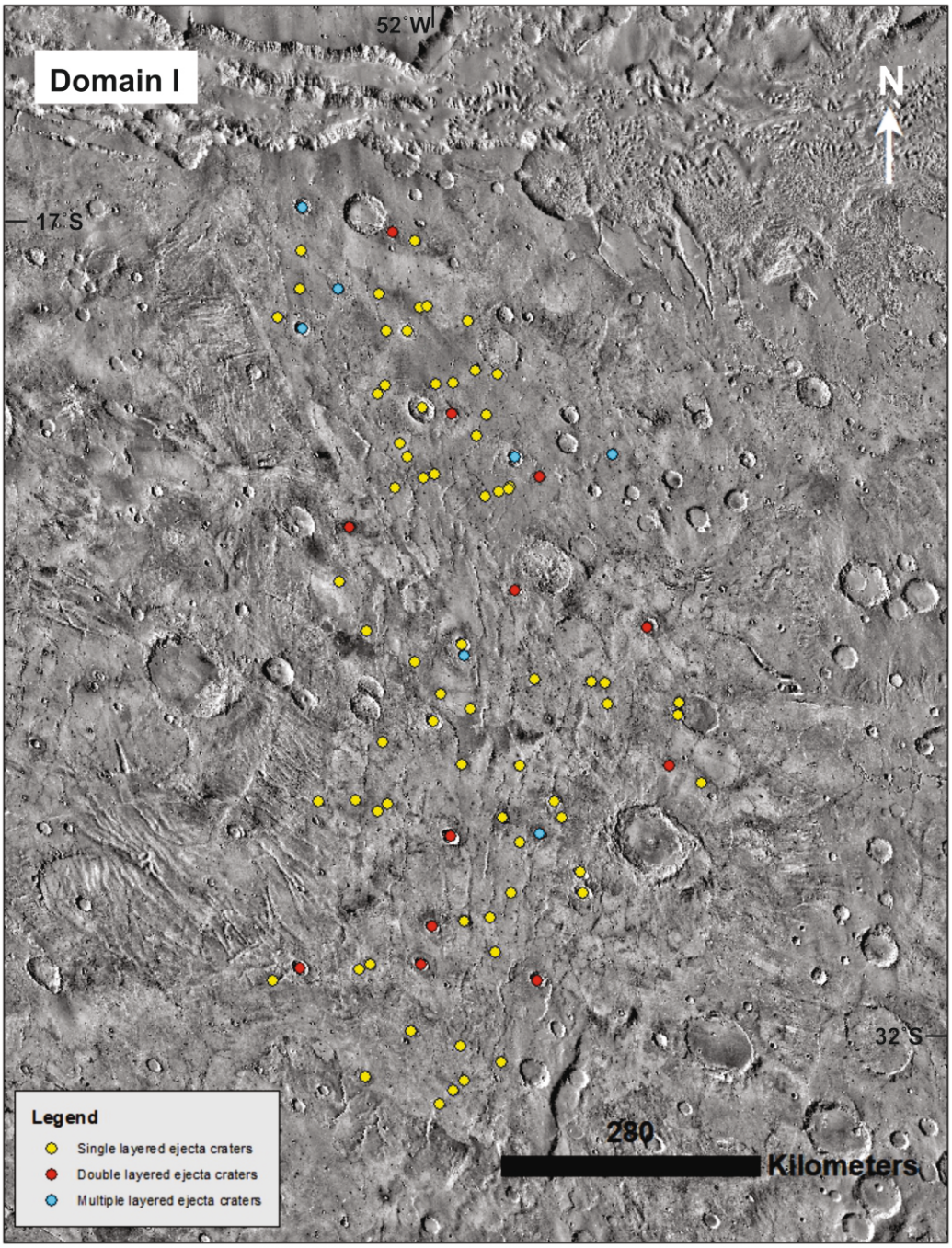

Figure 3c: THEMIS-IR Day Global Mosaic showing locations of different types of Layered ejecta crater in Domain I.

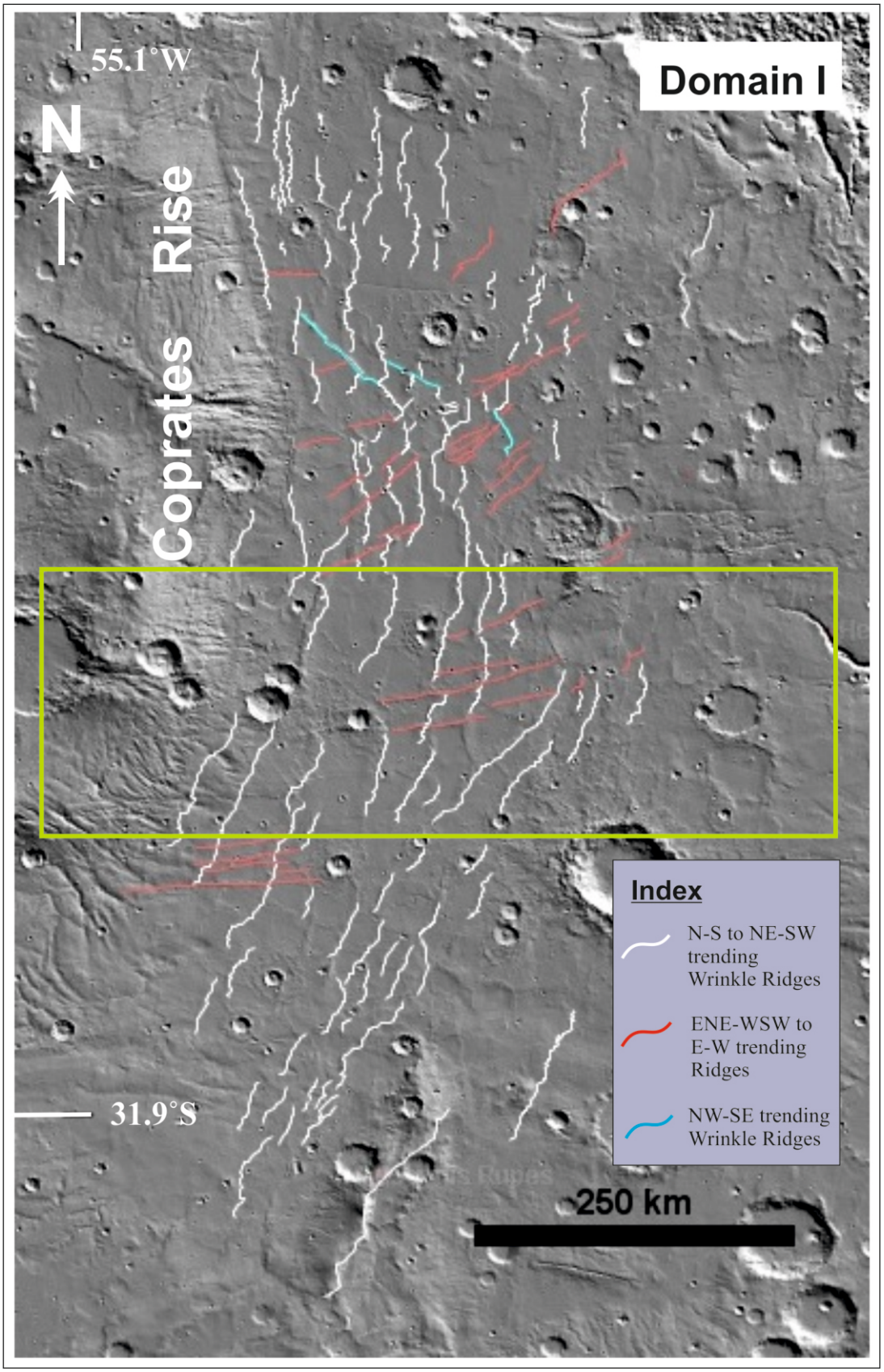

Figure 4: THEMIS-IR Day Global Mosaic showing ridges and wrinkle ridges of Domain I. Green rectangular box indicate the location of Figure 6a.

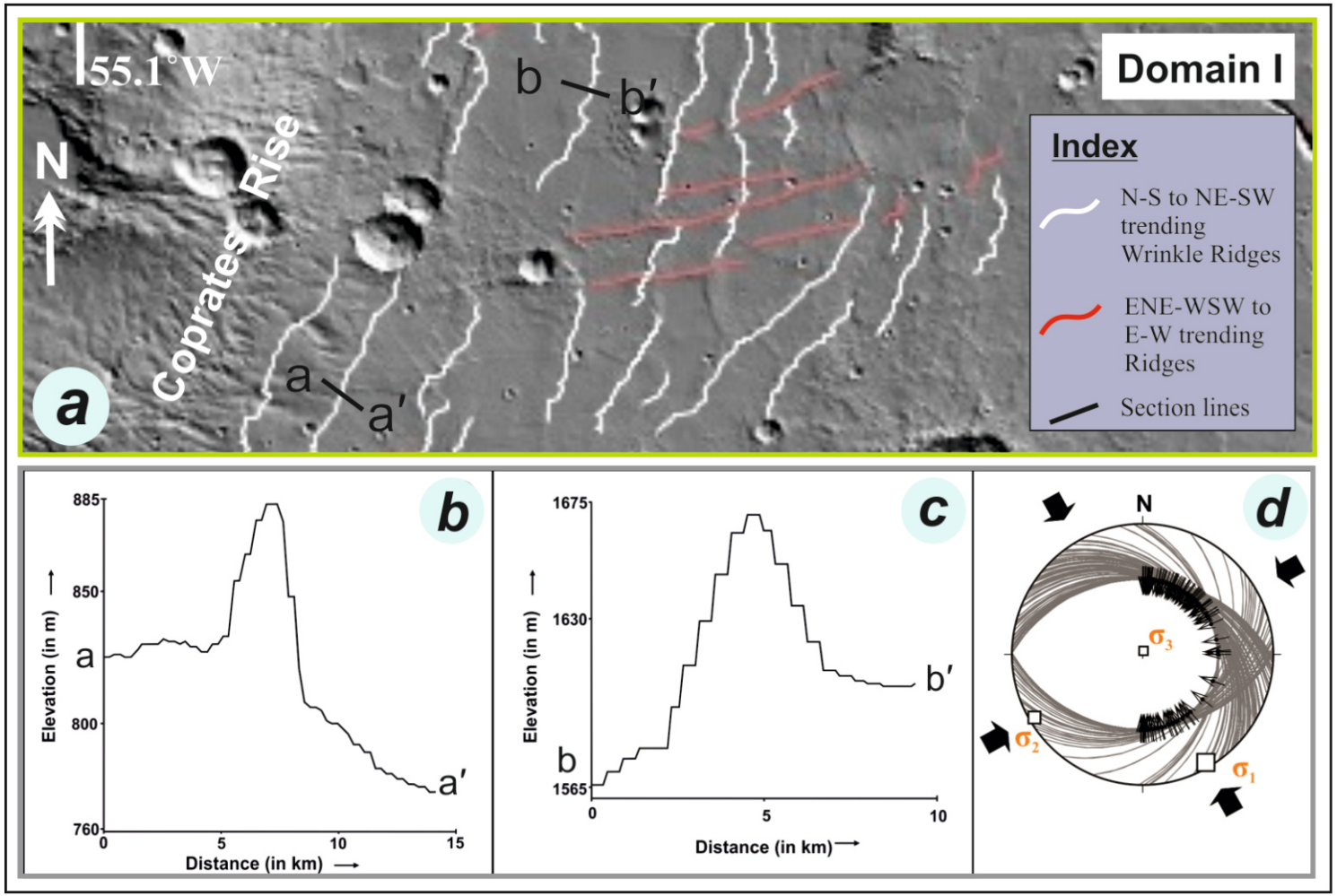

Figure 5: (a) Blown up image of Figure 5 (rectangular green box), **aa′** and **bb′** are the locations of wrinkle ridge profile sections; **(b)** Profile section of **aa′** extracted from MOLA DTM; **(c)** Profile section of **bb′** extracted from MOLA DTM; **(d)** Principal axes of stress (palaeostress) responsible for faulting that developed the N-S to NE-SW trending wrinkle ridges. The great circles represent the buried faults while arrows indicate slip-lines.

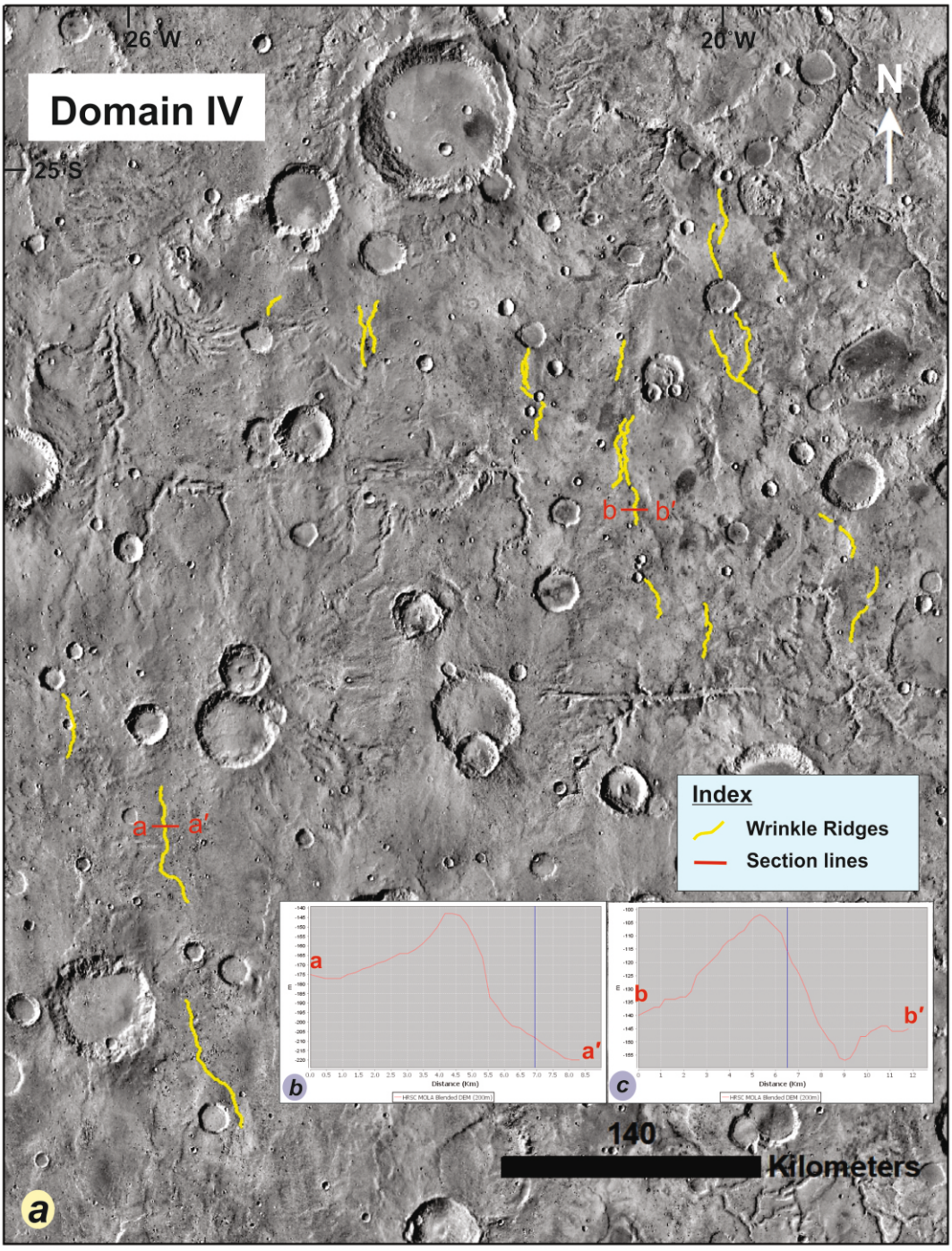

Figure 6: (a) Wrinkle ridges of domain IV; **aa′** and **bb′** are the locations of wrinkle ridge profile sections given in figure **(b)** and **(c)**,extracted from MOLA DTM .

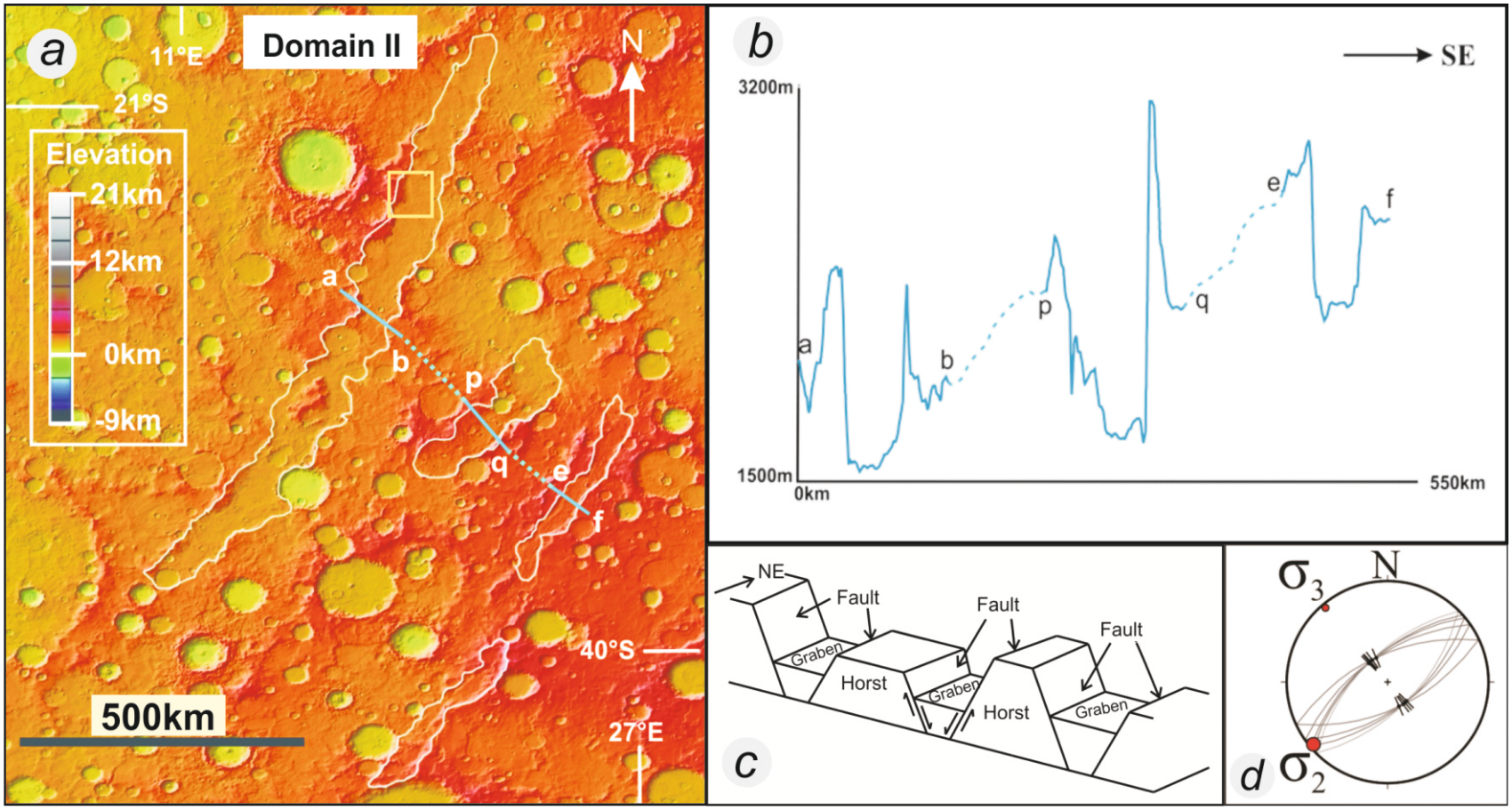

Figure 7: (a) MOLA colourized elevation image of Domain II, showing NNE-SSW trending grabens, marked by white irregular border. Section line is marked with blue line. Location of the pit chains (shown in Figure 9) is indicated by yellow box; **(b)** Profile section of the grabens marked by blue line in Figure a**; (c)** Schematic structure of the marked grabens of Figure a; **(d)** Paleostress condition of the grabens marked in Figure a.

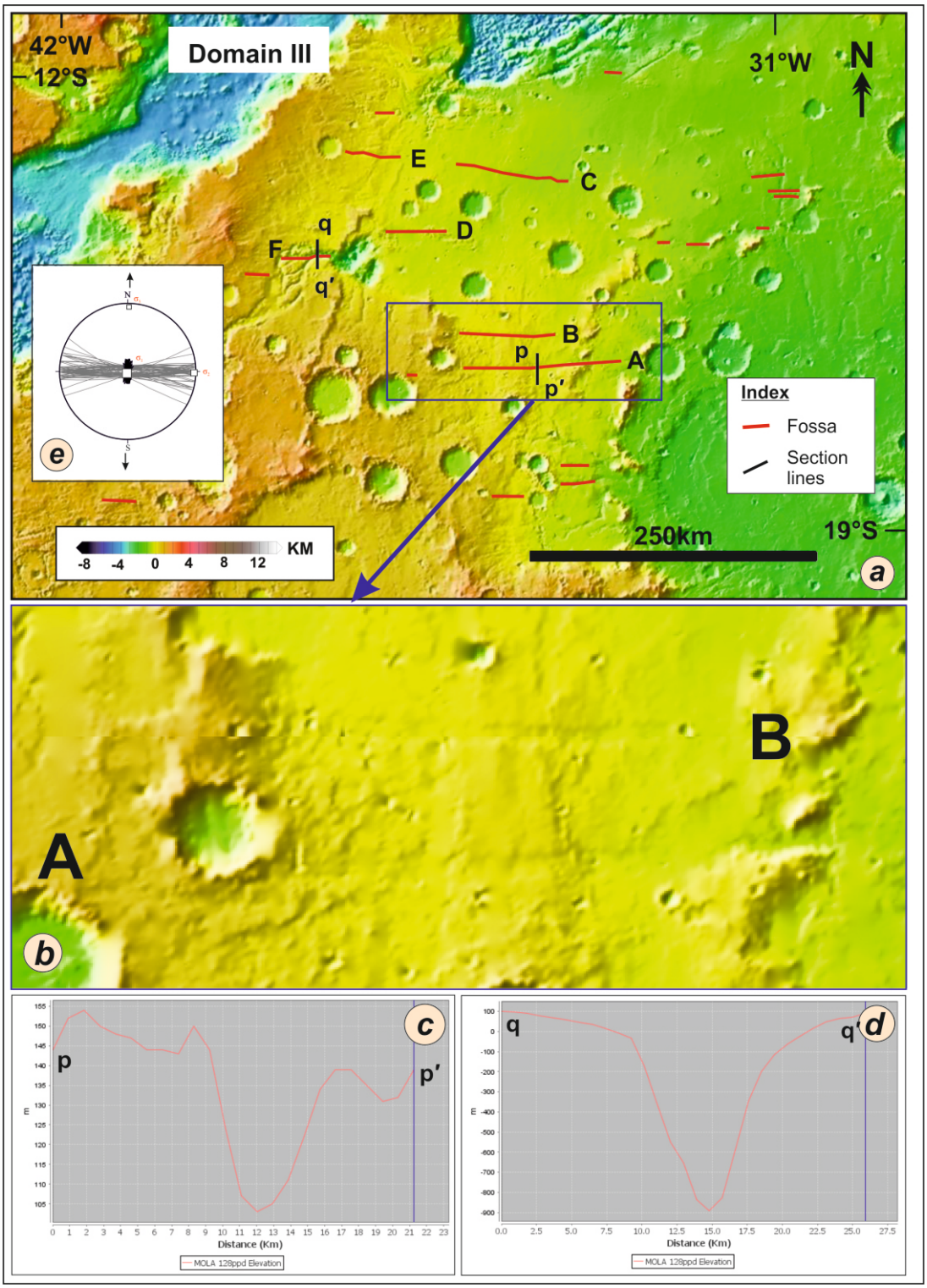

Figure 8: (a) MOLA Colourised elevation Map shows parallel fossae marked by red lines. Blown up image of Fossae A and B marked in blue rectangular box is shown in Figure **(b)**; Profile sections across fossae A and F are shown in Figure **(c)** and **(d)**, extracted from MOLA DTM; **(e)** Stereographic projection of fault planes and slips along the fault planes. The projection reveals vertical maximum principal stress (σ_1) and NS trending minimum principal stress (σ_3).

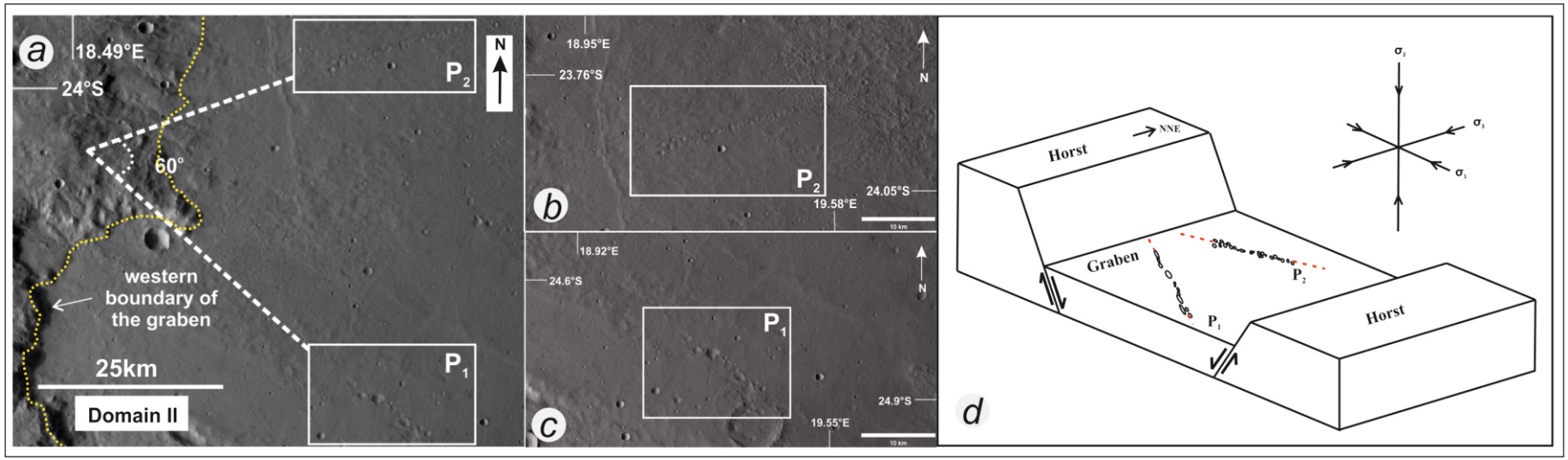

Figure 9: (a) Pit-crater chains within the westernmost graben of Figure 7.a. Yellow broken line indicates the western margin of the graben. Angle between the pit crater chains is shown; **(b)** Blown up image of WSW-ENE trending P_2 pit chain; **(c)** Blown up image of NW-SE trending P_1 Pit chain; **(d)** Stress condition responsible for the development of pit chains.

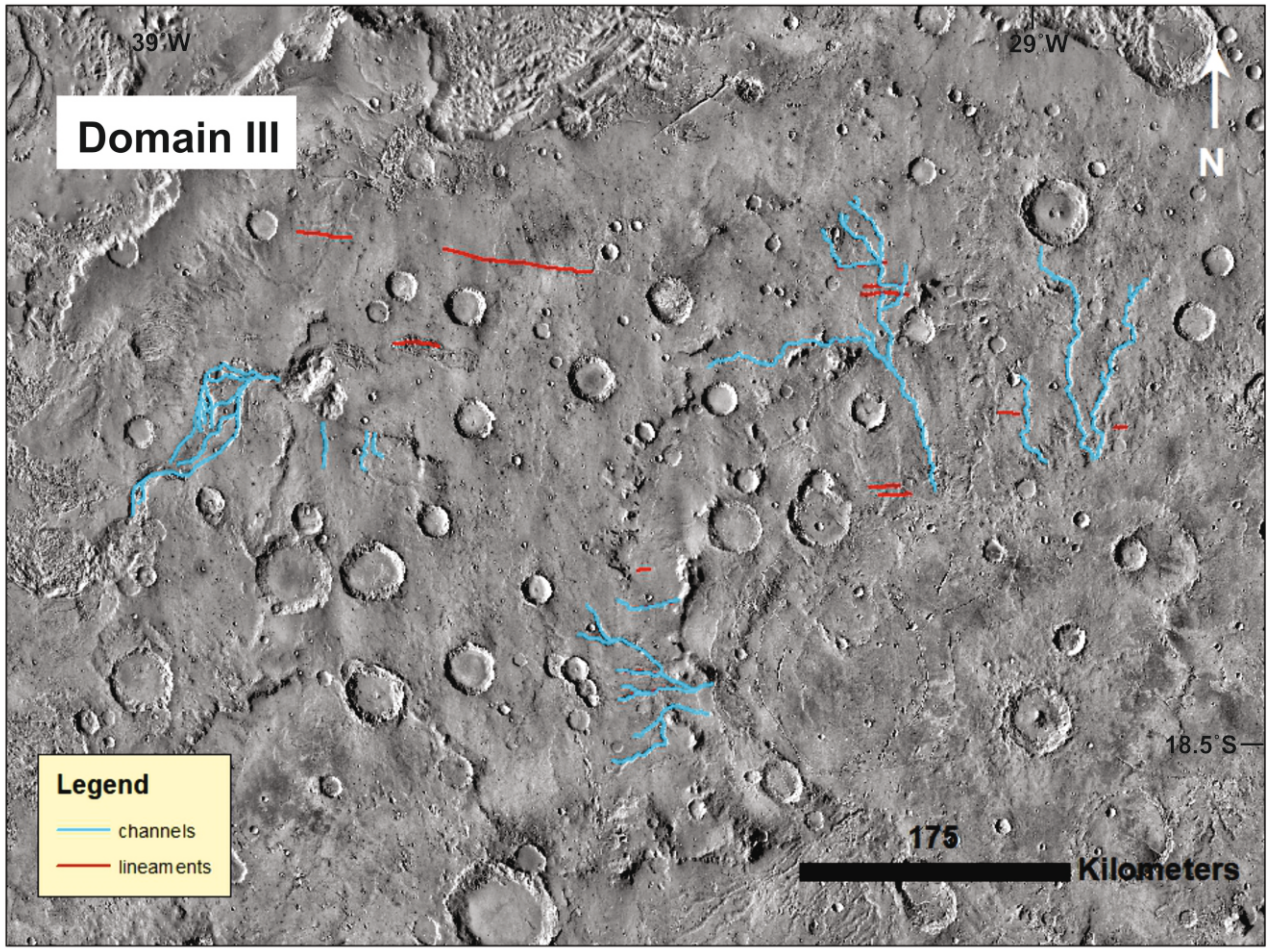

Figure 10: THEMIS-IR Day Global Mosaic showing channels and lineaments in Domain III. Channels show csimilar trend with lineaments in different part.

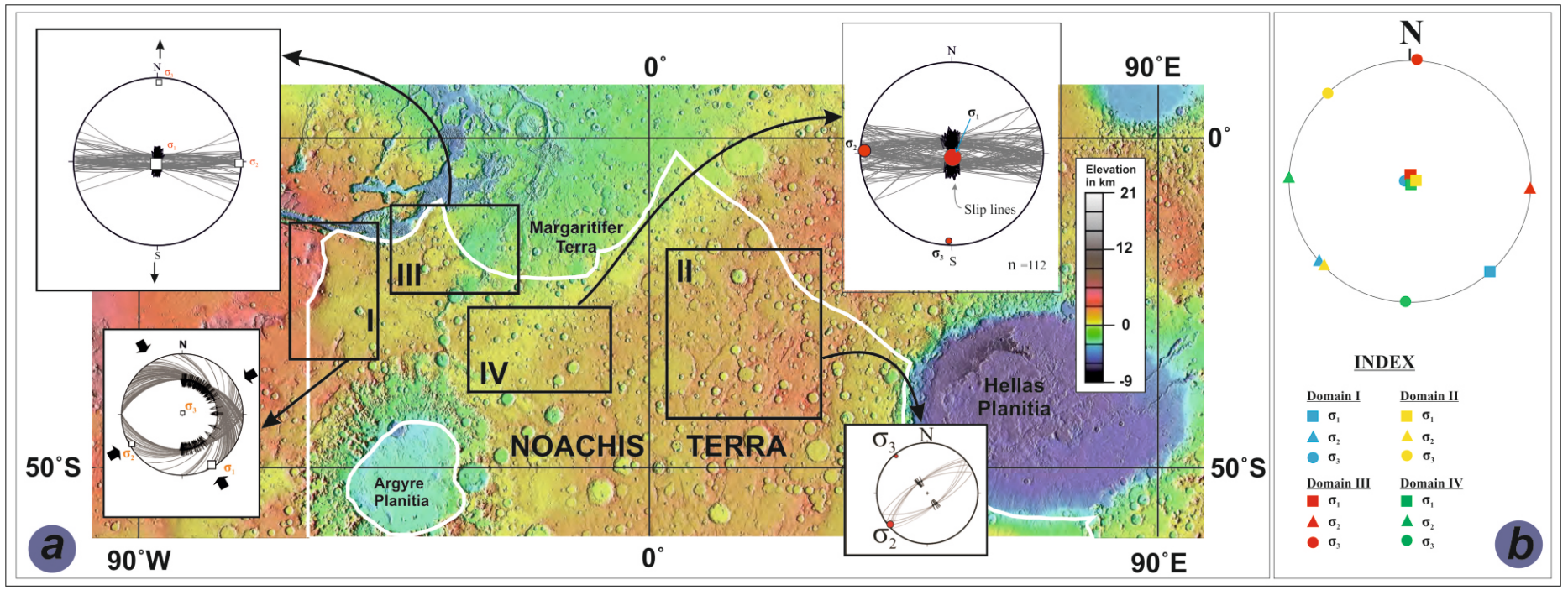

Figure 11: (a) Palaeostress conditions responsible for developing major structural elements in different domain of the area of study; **(b)** Stereographic projection of different palaeostress condition prevailed in different domain.

References:

Aittola, M., Öhman, T., Leitner, J.J. and Raitala, J., 2007. The characteristics of polygonal impact craters on Venus. Earth, Moon, and Planets, 101(1-2), pp.41-53. doi:10.1007/s11038-007-9148-4.

Aittola, M., Öhman, T., Leitner, J.J., Kostama, V.P. and Raitala, J., 2010. The structural control of Venusian polygonal impact craters. Icarus, 205(2), pp.356-363. doi:10.1016/j.icarus.2009.08.004.

Banerdt, W.B., Phillips, R.J., Sleep, N.H. and Saunders, R.S., 1982. Thick shell tectonics on one-plate planets: Applications to Mars. Journal of Geophysical Research: Solid Earth, 87(B12), pp.9723-9733.

Carr, M.H., 1996. Water on Mars. Oxford University Press, New York.

Christensen, P.R., Engle, E., Anwar, S., Dickenshied, S., Noss, D., Gorelick, N. and Weiss-Malik, M., 2009. JMARS-A Planetary GIS. In: Abstracts of the American Geophysical Union Fall Meeting, Abstract# IN22A-06.

Christensen, P.R., Jakosky, B.M., Kieffer, H.H., Malin, M.C., McSween, H.Y., Nealson, K., Mehall, G.L., Silverman, S.H., Ferry, S., Caplinger, M. and Ravine, M., 2004. The Thermal Emission Imaging System (THEMIS) for the Mars 2001 Odyssey mission. Space Science Reviews, 110(1-2), pp.85-130.

Davis, J.C., 2002. Statistics and data analysis in geology, third ed. John Wiley & Sons, New York.

De, K., Dasgupta, N. and Kundu, A., 2018. A statistical approach to decipher the tectonic control on the geometry of Martian channels: Case study from Pyrrhae

Fossae, Noachis Terra, Mars. Planetary and Space Science, (article in press). doi:10.1016/j.pss.2018.07.006.

De, K., Dasgupta, N., Kundu, A. and Chauhan, P., 2015b. Fluvial channels in the north-western part of Noachis Terra, Mars: Implications for tectonic controls. In: Abstracts of 10th European Planetary Science Congress, Abstract# EPSC2015_296.

De, K., Kundu, A., Chauhan, P. and Dasgupta, N., 2015a. An example of consistent palaeostress regime resulting in morphometric irregularity in the northwestern part of Noachis Terra, Mars. Current Science, 108(12), pp.2156-2159.

De, K., Kundu, A., Chauhan, P., Ruj, T. and Dasgupta, N., 2014. Pit-crater chains within a graben in Noachis Terra, Mars. Proceedings of Rock Deformation and Structure, 3, pp. 89-90.

Edwards, C.S., Nowicki, K.J., Christensen, P.R., Hill, J., Gorelick, N. and Murray, K., 2011. Mosaicking of global planetary image datasets: 1. Techniques and data processing for Thermal Emission Imaging System (THEMIS) multi-spectral data. Journal of Geophysical Research: Planets, 116(E10). doi:10.1029/2010JE003755.

Eppler, D.T., Ehrlich, R., Nummedal, D. and Schultz, P.H., 1983. Sources of shape variation in lunar impact craters: Fourier shape analysis. Geological Society of America Bulletin, 94(2), pp.274-291. doi: 10.1130/0016-7606(1983)94<274:SOSVIL>2.0.CO;2.

Fergason, R.L., Hare, T.M. and Laura, J., 2018. HRSC and MOLA Blended Digital Elevation Model at 200m v2. Astrogeology PDS Annex. U.S. Geological Survey, URL: http://bit.ly/HRSC_MOLA_Blend_v0.

Ferrill, D.A., Wyrick, D.Y., Morris, A.P., Sims, D.W. and Franklin, N.M., 2004. Dilational fault slip and pit chain formation on Mars. GsA Today, 14(10), pp.4-12. doi: 10.1130/10525173(2004)014<4:DFSAPC>2.0.CO;2.

Gault, D.E., Quaide, W.L. and Oberbeck, V.R., 1968. Impact cratering mechanics and structures. In: French, B.M., Short, N.M. (eds.), Shock metamorphism of natural materials, Mono Book Corporation.

Golombek, M. P., Tanaka, K. L. and Franklin, B. J., 1996. Extension across Tempe Terra, Mars, from measurements of fault scarp widths and deformed craters. Journal Geophysical Research, 101, pp.26119-26130.

Gravelius, H., 1914. Flusskunde. Goschen Verlagshandlung, Berlin.

Grott, M., Hauber, E., Werner, S.C., Kronberg, P. and Neukum, G., 2007. Mechanical modeling of thrust faults in the Thaumasia region, Mars, and implications for the Noachian heat flux. Icarus, 186(2), pp.517-526.

Güneralp, İ. and Rhoads, B.L., 2005. The spatial structure of planform dynamics of meandering rivers. In: Abstracts of IAHR Symposium on River, Coastal and Estuarine Morphodynamics. International Association of Hydraulic Engineering and Research, Urbana, IL.

Holcombe, R.J., 2005. GEOrient 9.2. www.holcombe.net.au/software/. [online]. Department of Earth sciences, The University of Queensland.

Hynek, B.M., Beach, M. and Hoke, M.R., 2010. Updated global map of Martian valley networks and implications for climate and hydrologic processes. Journal of Geophysical Research: Planets, 115(E9). doi:10.1029/2009JE003548.

Jaumann, R., Neukum, G., Behnke, T., Duxburry, T.C., Eichentopf, K., Gasselt, S.V., Giese, B., Gwinner, K., Hauber, E., Hoffmann, H., Hoffmeister, A., Köhler, U.,

Matz, K.D., McCord, T.B., Mertens, V., Oberst, J., Pischel, R., Reiß, D., Ress, E., Roatsch, T., Saiger, P., Scholten, F., Schwarz, G., Stephan, K., Wählisch, M. and the HRSC Co-Investigator Team, 2007. The High Resolution Stereo Camera (HRSC) Experiment on Mars Express: Instrument Aspects and Experiment Conduct from Interplanetary Cruise through Nominal Mission. Planetary and Space Science, 55, pp.928-952.

Kochel, R.C. and Piper, J.F., 1986. Morphology of large valleys on Hawaii: Evidence for groundwater sapping and comparisons with Martian valleys. Journal of Geophysical Research: Solid Earth, 91(B13), pp. E175-E192.

Komatsu, G. and Baker, V.R., 2007. Formation of valleys and cataclysmic flood channels on Earth and Mars, In: Chapman, M.G. (ed.), The geology of Mars: Evidence from earth-based analogs. Cambridge University Press, New York, pp. 297-321.

Korteniemi, J. and Öhman, T., 2014. Polygonal Crater. In: Encyclopedia of Planetary Landforms. Springer, New York.

Korteniemi, J., Aittola, M., Öhman, T. and Raitala, J., 2006. Floor-fractured craters on the terrestrial planets – The Martian perspective. In: Wilson A. (ed.): Proceedings, 40th SLAB – First International Conference on Impact Cratering in the Solar System, ESA Special Publication SP-612, pp. 193-198.

Laity, J.E. and Malin, M.C., 1985. Sapping processes and the development of theater-headed valley networks on the Colorado Plateau. Geological Society of America Bulletin, 96(2), pp.203-217.

Li, L., Yue, Z., Di, K. and Peng, M., 2015. Observations of Martian layered ejecta craters and constraints on their formation mechanisms. Meteoritics & Planetary Science, 50(3), pp.508-522.

Lucchitta, B.K., McEwen, A. S., Clow, C. D., Geissler, R.B., Singer, R. B., Schultz, R. A., and Squyres, S.W., 1992. The canyon system on Mars. In Mars, ed. H. H. Kieffer, B. M. Jakosky, C.W. Snyder and M. S. Matthews. Tucson, AZ: University of Arizona Press.

Malin, M.C., Bell, J.F., Cantor, B.A., Caplinger, M.A., Calvin, W.M., Clancy, R.T., Edgett, K.S., Edwards, L., Haberle, R.M., James, P.B. and Lee, S.W., 2007. Context camera investigation on board the Mars Reconnaissance Orbiter. Journal of Geophysical Research: Planets, 112(E5). doi:10.1029/2006JE002808.

Mangold, N., Adeli, S., Conway, S., Ansan, V. and Langlais, B., 2012. A chronology of early Mars climatic evolution from impact crater degradation. Journal of Geophysical Research: Planets, 117(E4). doi:10.1029/2011JE004005.

Mangold, N., Quantin, C., Ansan, V., Delacourt, C., Allemand, P., 2004. Evidence for precipitation on Mars from dendritic valleys in the Valles Marineris area. Science 305(5680), pp.78-81. doi: 10.1126/science.1097549.

McEwen, A.S., Eliason, E.M., Bergstrom, J.W., Bridges, N.T., Hansen, C.J., Delamere, W.A., Grant, J.A., Gulick, V.C., Herkenhoff, K.E., Keszthelyi, L. and Kirk, R.L., 2007. Mars reconnaissance orbiter's high resolution imaging science experiment (HiRISE). Journal of Geophysical Research: Planets, 112(E5).

Montési, L.G. and Zuber, M.T., 2003. Clues to the lithospheric structure of Mars from wrinkle ridge sets and localization instability. Journal of Geophysical Research: Planets, 108(E6).

Mustard, J. F., Poulet, F., Gendrin, A., Bibring, J.-P., Langevin, Y., Gondet, B., Mangold, N., Bellucci, G. and Altieri , F., 2005. Olivine and Pyroxene Diversity in the Crust of Mars. Science, 307.

Neukum, G., Jaumann, R. and the HRSC Co-Investigator and Experiment Team, In Mars Express: The Scientific Payload, (ed. Wilson, A., scientific contribution: Chicarro, A.), European Space Agency Special Publication, SP-1240, Noordwijk, The Netherlands, 2004, pp. 17-35.

Öhman, T., Aittola, M., Kostama, V.P. and Raitala, J., 2005. The preliminary analysis of polygonal impact craters within greater Hellas region, Mars. In: Koeber, C., Henkel, H. (eds), Impact tectonics, Springer, Berlin, pp. 131-160.

Öhman, T., Aittola, M., Kostama, V.P., Raitala, J. and Korteniemi, J., 2008. Polygonal impact craters in Argyre region, Mars: Implications for geology and cratering mechanics. Meteoritics and Planetary Science, 43(10), pp.1605-1628.

Poelchau, M.H., Kenkmann, T. and Kring, D.A., 2009. Rim uplift and crater shape in Meteor Crater: Effects of target heterogeneities and trajectory obliquity. Journal of Geophysical Research: Planets, 114(E1).

Robbins, S.J., Hynek, B.M., Lillis, R.J. and Bottke, W.F., 2013. Large impact crater histories of Mars: The effect of different model crater age techniques. Icarus, 225(1), pp.173-184.

Ruj, T., Komatsu, G., Dohm, J.M., Miyamoto, H. and Salase, F., 2016. Effect of the Hellas impact on regional tectonism: A case study from the Noachis-Sabaea region, southern highlands of Mars. In: Abstracts of the 47th Lunar and Planetary Science Conference, Abstract# 1512.

Ruj, T., Komatsu, G., Dohm, J.M., Miyamoto, H. and Salese, F., 2017. Generic identification and classification of morphostructures in the Noachis-Sabaea region, southern highlands of Mars. Journal of Maps, 13(2), pp.755-766.

Ruj, T., Komatsu, G., Pasckert, J.H. and Dohm, J.M., 2018. Timings of early crustal activity in southern highlands of Mars: Periods of crustal stretching and shortening. Geoscience Frontiers.

Schultz, R. A., 2000. Localization of bedding plane slip and backthrust faults above blind thrust faults: Keys to wrinkle ridge structure. Journal of Geophysical Research, 105(E5), pp.12,035-12,052.

Schultz, R.A., 1989. Strike-slip faulting of ridged plains near Valles Marineris, Mars. Nature, 341(6241), pp.424-426.

Sharp, R.P. and Malin, M.C., 1975. Channels on mars. Geological Society of America Bulletin, 86(5), pp.593-609.

Smith, D.E., Zuber, M.T., Frey, H.V., Garvin, J.B., Head, J.W., Muhleman, D.O., Pettengill, G.H., Phillips, R.J., Solomon, S.C., Zwally, H.J. and Banerdt, W.B., 2001. Mars Orbiter Laser Altimeter: Experiment summary after the first year of global mapping of Mars. Journal of Geophysical Research: Planets 106(E10), pp. 23689-23722.

Tanaka, K.L., Skinner, J.A. Jr., Dohm, J.M., Irwin, R.P. III., Kolb, E.J., Fortezzo, C.M., Platz, T., Michael, G.G. and Hare, T.M., 2014. Geologic map of Mars: U.S. Geological Survey Scientific Investigations Map 3292, scale 1:20,000,000, pamphlet 2014. http://dx.doi.org/10.3133/sim3292.

Telatovich, E.R., 1998. Correlation data as an aid in fault interpretation: a case study. Geological Society of Malaysia Bulletin, 42, 27–37.

Watters, T. R., and Schultz, R. A., 2010. Planetary Tectonics. Cambridge University Press, pp.183-232.

Watters, T.R. and Robinson, M.S., 1997. Radar and photoclinometric studies of wrinkle ridges on Mars. Journal of Geophysical Research: Planets, 102(E5), pp.10889-10903.

Watters, W.A., Geiger, L.M., Fendrock, M., Gibson, R. and Hundal, C.B., 2017. The role of strength defects in shaping impact crater planforms. Icarus 286, 15–34.

Watters, W.A., Grotzinger, J.P., Bell, III. J., Grant, J., Hayes, A.G., Li, R., Squyres, S.W. and Zuber, M.T., 2011. Origin of the structure and planform of small impact craters in fractured targets: Endurance Crater at Meridiani Planum, Mars. Icarus 211(1), pp.472-497.

Werner, S.C., 2008. The early Martian evolution—Constraints from basin formation ages. Icarus, 195(1), pp.45-60.

Wilhelms, D.E. and Squyres, S.W., 1984. The Martian hemispheric dichotomy may be due to a giant impact. Nature, 309(5964), p.138.

Williams, D.A., Greeley, R., Werner, S.C., Michael, G., Crown, D.A., Neukum, G. and Raitala, J., 2008. Tyrrhena Patera: geologic history derived from Mars express high resolution stereo camera. Journal of Geophysical Research: Planets, 113(E11).

Wilson, L. and Head, J. W., 2002. Tharsis-radial graben systems as the surface manifestation of plume-related dike intrusion complexes: Models and implications. Journal of Geophysical Research, 107(E8), Doi:10.1029/2001JE001593.

Witbeck, N. E., Tanaka, K. L., and Scott, D. H., 1991. Geologic map of the Valles Marineris region, Mars (East Half And West Half): 1:2M. U.S. Geol. Surv. Misc. Invest. Ser., Map I-2010.

Wyatt, M.B. and McSween Jr, H.Y., 2002. Spectral evidence for weathered basalt as an alternative to andesite in the northern lowlands of Mars. Nature, 417(6886), p.263.

Wyrick, D., Ferrill, D. A., Morris, A. P., Colton, S. L. and Sims, D. W., 2004. Journal of Geophysical Research, 109, E06005; doi: 10.1029/2004JE002240.

Xiao, L., Huang, J., Christensen, P.R., Greeley, R., Williams, D.A., Zhao, J. and He, Q., 2012. Ancient volcanism and its implication for thermal evolution of Mars. Earth and Planetary Science Letters, 323, pp.9-18.

Žalohar, J., 2009. T-TECTO 3.0 Professional. Integrated software for structural analysis of fault-slip data. Department of Geology, SI-1000 Ljubljana, Slovenia.

Zavoianu, I., 1985. Morphometry of drainage basins, first ed. Elsevier Science, Amsterdam.

Zernitz, E.R., 1932. Drainage patterns and their significance. The Journal of Geology, 40(6), pp.498-521.